Journal of Clinical and Translational Hepatology **2026** vol. 14(2) | 187–201
DOI: 10.14218/JCTH.2025.00592

Original Article

Cathepsin K Alleviates Liver Fibrosis by Inhibiting the TGF-β/Smad Signaling Pathway and Inducing Hepatic Stellate Cell Apoptosis

Zhandong Lin, Yue Shi, Mengjiao Sun, Jiawei Cui, Dandan Zhao, Yaoyao Mao, Congyue Zhang, Ying Zhang, Qianqian Zheng, Yukai Chen, Shaoya Li and Yuemin Nan*

Department of Traditional and Western Medical Hepatology, Hebei Provincial Key Laboratory of Liver Fibrosis in Chronic Liver Diseases, Hebei Medical University Third Hospital, Shijiazhuang, Hebei, China

Received: November 07, 2025 | **Revised:** December 19, 2025 | **Accepted:** December 31, 2025 | **Published online:** January 22, 2026

Abstract

Background and Aims: Liver fibrosis is characterized by the excessive deposition of extracellular matrix, a process primarily driven by activated hepatic stellate cells (HSCs), and currently lacks effective therapy. Cathepsin K (CTSK) exhibits context-dependent roles across organ systems in fibrosis, but its function in liver fibrosis is unclear. This study aimed to investigate the role and underlying mechanisms of CTSK during liver fibrosis. ***Methods:*** CTSK expression was analyzed in human fibrotic liver samples via transcriptomic analysis and confirmed in murine fibrosis models. The function of CTSK was investigated in both primary HSCs and LX-2 cells by assessing its effects on cell activation, proliferation, apoptosis, and the underlying signaling pathways following CTSK overexpression. The therapeutic potential was evaluated using an adeno-associated virus serotype 8 to overexpress CTSK in two etiologically distinct murine fibrosis models. ***Results:*** CTSK was upregulated in activated HSCs and fibrotic livers. Furthermore, we discovered that it mediates a negative feedback loop to inhibit the TGF-β/Smad pathway via Smad7/Smurf2-dependent TGF-β receptor-I degradation, thereby suppressing HSC activation and proliferation. CTSK also induced mitochondrial apoptosis through Bax/Bcl-2 imbalance and caspase-3 activation. Together, these actions contribute to the anti-fibrotic effect of CTSK. Notably, adeno-associated virus serotype 8-mediated CTSK overexpression attenuated liver fibrosis across multiple murine models. ***Conclusions:*** Our study demonstrates that elevated CTSK functions as an endogenous protective factor that attenuates liver fibrosis. CTSK mediates negative feedback inhibition of the TGF-β pathway while concurrently promoting the mitochondrial apoptosis pathway. The dual anti-fibrotic mechanisms identify CTSK as a promising therapeutic target for liver fibrosis.

Citation of this article: Lin Z, Shi Y, Sun M, Cui J, Zhao D, Mao Y, *et al*. Cathepsin K Alleviates Liver Fibrosis by Inhibiting the TGF-β/Smad Signaling Pathway and Inducing Hepatic Stellate Cell Apoptosis. J Clin Transl Hepatol 2026;14(2):187–201. doi: 10.14218/JCTH.2025.00592.

Keywords: Liver fibrosis; Hepatic stellate cell; TGF-β/Smad signaling; Cathepsin K; Bax/Bcl-2 balance; Apoptosis.

***Correspondence to:** Yuemin Nan, Department of Traditional and Western Medical Hepatology, Hebei Medical University Third Hospital, 139 Ziqiang Road, Shijiazhuang, Hebei 050051, China. ORCID: https://orcid.org/0000-0003-4192-099X. Tel: +86-18533112266, Fax: +86-311-66781289, E-mail: nanyuemin@hebmu.edu.cn or nanyuemin@163.com.

Introduction

Liver fibrosis is a pathological consequence of chronic liver injury, characterized by the excessive deposition and impaired degradation of collagen-rich extracellular matrix.[1] The progression of chronic liver fibrosis to cirrhosis and hepatocellular carcinoma constitutes a substantial and growing global health burden.[2] To date, no effective antifibrotic medications have been approved.[3] This therapeutic gap necessitates a comprehensive understanding of the pathogenesis of hepatic fibrosis to identify novel therapeutic targets to halt fibrotic progression in chronic liver injury.

The activation of quiescent, vitamin A–storing HSCs into profibrogenic myofibroblasts represents the central driver of liver fibrosis.[4] This transformation is orchestrated by multiple signaling pathways, with TGF-β serving as a master regulator of HSC activation. In the canonical TGF-β–Smad2/3 pathway, TGF-β induces Smad2/3 activation through TGF-β receptor I/II (TβR-I/II). Subsequently, the phosphorylated Smad2/3 translocates into the nucleus and activates or represses target genes.[5] Targeting the pleiotropic TGF-β has proven exceptionally challenging due to its critical roles in homeostasis and immunity.[6] This impasse requires identifying precise, context-specific nodes in the TGF-β signaling network that can be safely targeted. TβRs mediate extracellular stimuli to intracellular responses, so their distribution and stability are critical for TGF-β signaling transduction.[7] The ubiquitin–proteasome system (UPS) is a critical mediator of protein turnover and signal transduction.[8] Notably, the Smad7/Smurf2 axis, an established negative feedback mechanism that targets the TβRs for ubiquitination and degradation,[9,10] presents an attractive but poorly understood target for precise therapeutic intervention in liver fibrosis.

CTSK, initially characterized for its role in bone resorption,[11] is now recognized as a multifunctional regulator involved in various pathological conditions. CTSK can protect against chronic intestinal inflammation via its antimicrobial function.[12] Moreover, it is reported that CTSK is associated

with obesity and atherogenesis,[13,14] indicating a potential role of CTSK in lipid metabolism. Recently, evidence indicates that CTSK promotes the ubiquitination and subsequent degradation of specific protein substrates by recruiting E3 ubiquitin ligases.[15–17] Notably, CTSK exhibits tissue-specific roles in fibrosis across different organ systems: it acts as an anti-fibrotic in the heart and lungs,[18,19] yet paradoxically accelerates fibrosis in the kidney.[20] Although CTSK is upregulated in human liver fibrosis,[21] it remains unknown whether this represents a maladaptive driver of disease or a host-protective response.

Our study sought to define the role of CTSK in HSCs during liver fibrosis. We demonstrate that CTSK functions as an endogenous protective factor that represses HSC activation and proliferation. Mechanistically, CTSK inhibits TGF-β/Smad signaling by promoting Smad7/Smurf2 axis–mediated ubiquitination and degradation of TβR-I. Concurrently, CTSK can trigger the mitochondrial pathway of apoptosis in HSCs. These findings extend our understanding of CTSK in liver disease and establish it as a promising molecular target for anti-fibrotic therapy.

Methods

Mouse liver fibrosis induction and treatment

Male C57BL/6J mice (eight weeks old) were purchased from HFK Bioscience (Beijing, China) and housed under controlled humidity and temperature conditions with a 12-h light/dark cycle. All procedures were conducted in accordance with the guidelines of the Animal Care and Use Committee of Hebei Province and were approved by the Animal Experiment Ethics Committee of the Third Hospital of Hebei Medical University. The overexpression of CTSK was mediated by transduction of a liver-specific adeno-associated virus serotype (AAV) 8 vector in mouse models of carbon tetrachloride (CCl_4) attack or bile duct ligation (BDL) surgery. The CTSK coding sequence was amplified by PCR and cloned into an AAV vector under the control of a CMV promoter with a C-terminal 3×FLAG tag. The recombinant AAV genome was then packaged into AAV8 capsids to produce the AAV8-CTSK virus (AAV8-CTSK-3×FLAG, denoted as AAV8-CTSK).[22] This virus, along with the AAV8-Scramble control virus (denoted as AAV8-vector), was obtained from HanBio (Shanghai, China).

CCl_4-induced model: After one week of acclimatization, male mice were randomly divided into four experimental groups (n = 6): (1) Oil+AAV8-vector (Oil+vector), (2) Oil+AAV8-CTSK (Oil+oeCTSK), (3) CCl_4+AAV8-vector (CCl_4+vector), and (4) CCl_4+AAV8-CTSK (CCl_4+oeCTSK). Liver fibrosis was induced by intraperitoneal (i.p.) injection of CCl_4 (1:10 v/v dilution in olive oil) at a dosage of 5 mL/kg body weight, administered twice per week for 6 weeks.[23] At the beginning of the third week, mice received a tail vein injection of AAV8-vector or AAV8-CTSK (1×10^{11} vg/mouse in 100 μL saline).

BDL-induced model: After one week of acclimatization, male mice were randomly divided into four experimental groups (n = 6): (1) Sham+AAV8-vector (Sham+vector), (2) Sham+AAV8-CTSK (Sham+oeCTSK), (3) BDL+AAV8-vector (BDL+vector), and (4) BDL+AAV8-CTSK (BDL+oeCTSK). Two weeks after receiving the AAV8 injection (1×10^{11} vg/mouse in 100 μL saline), mice were anesthetized and subjected to BDL or sham surgery as previously described.[24] Briefly, for the BDL group, the common bile duct was double-ligated with silk suture and transected between the ligatures. For sham-operated controls, the bile duct was exposed but not ligated or transected. Liver tissues and serum samples were collected on postoperative day 14 for subsequent analysis.

Primary mouse HSCs (pHSCs) isolation and transfection

pHSCs were isolated using the collagenase perfusion method as previously described.[25] The liver was initially perfused with 30 mL of perfusate solution (NaCl 8,000 mg/L, KCl 400 mg/L, NaH_2PO_4 88.17 mg/L, Na_2HPO_4 120.45 mg/L, HEPES 2,380 mg/L, $NaHCO_3$ 350 mg/L, EGTA 190 mg/L, glucose 900 mg/L, pH 7.35–7.40) through the inferior vena cava. The liver was then perfused with 35 mL of enzyme buffer (NaCl 8,000 mg/L, KCl 400 mg/L, NaH_2PO_4 88.17 mg/L, Na_2HPO_4 120.45 mg/L, HEPES 2,380 mg/L, $NaHCO_3$ 350 mg/L, $CaCl_2$ 560 mg/L, pH 7.35–7.40) containing 14 mg pronase. Finally, the liver was perfused with 40 mL of enzyme buffer containing 19.17 mg collagenase IV. After isolation via discontinuous Percoll gradient centrifugation (25%–50%), pHSCs were seeded in 12-well plates at 2×10^5 cells/well and cultured in complete DMEM (10% FBS, 1% penicillin-streptomycin) at 37 °C with 5% CO_2. Recombinant adenoviruses expressing CTSK or a scrambled control sequence were transduced into pHSCs to overexpress CTSK. Recombinant adenoviruses were obtained from HanBio.

Human HSC line LX-2 cells culture and transfection

LX-2 cells (Pricella, Wuhan, China; Cat. # CL-0560), a human HSC line, were cultured in DMEM containing 10% FBS and 1% penicillin-streptomycin at 37 °C in a 5% CO_2 atmosphere. For transient transfection, cells were seeded in appropriate plates and transfected at 60%–70% confluence using Lipofectamine™ 3000 reagent according to the manufacturer's instructions.[26] The pcDNA3.1-CTSK plasmid and its corresponding empty vector were obtained from GenePharma (Shanghai, China). The HA-tagged pcDNA3.1-ubiquitin plasmid and its corresponding empty vector were obtained from GENCEFE (Jiangsu, China). Three siRNAs targeting Smad7 and a negative control siRNA were obtained from GENCEFE, as detailed in Supplementary Table 1. For TGF-β1 treatment, cells were serum-starved for 24 h and then stimulated with 5 ng/mL recombinant human TGF-β1.[27]

Histopathology examination and immunohistochemistry

For histological analysis, mouse liver specimens were fixed, paraffin-embedded, and sectioned. After deparaffinization and rehydration, staining was performed as follows: H&E with hematoxylin and eosin; Masson's Trichrome with Biebrich Scarlet-Acid Fuchsin and aniline blue; Sirius Red with Sirius red solution. All stained sections were then dehydrated and coverslipped. For immunohistochemistry, prepared sections underwent peroxidase blocking with H_2O_2, antigen retrieval in citrate buffer, blocking with BSA, and sequential incubation with primary (4 °C, overnight) and secondary antibodies. Signals were detected with DAB. Fibrosis was quantified by measuring the collagen-positive area using ImageJ, expressed as a percentage of the total area.[28]

Immunofluorescence staining

For cell immunofluorescence, cells on coverslips were fixed with 4% paraformaldehyde (15 min), permeabilized with 0.3% Triton X-100 (10 min), and blocked with 5% BSA (30 min). After incubation with primary antibodies (4 °C, overnight) and fluorescent secondary antibodies (Invitrogen; 37 °C, 1 h), nuclei were stained with DAPI. For liver section immunofluorescence, paraffin-embedded liver sections

were deparaffinized, rehydrated, and subjected to antigen retrieval in citrate buffer. After blocking with BSA, the sections were incubated sequentially with the primary antibody (4 °C, overnight) and the secondary antibody. Nuclei were stained with DAPI. Apoptosis was detected using a One Step TUNEL Apoptosis Assay Kit (Beyotime, China; Cat. # C1086) strictly according to the manufacturer's instructions. Cells were processed identically through permeabilization before incubation with the reaction mixture (37°C, 1 h, dark).[29] All fluorescent images were acquired using an Olympus microscope and analyzed with ImageJ. Colocalization between signals from the two fluorescence channels was quantified by calculating Pearson's correlation coefficient using the JACoP plugin in ImageJ.[30]

Western blot analysis

Liver tissues or cells were lysed on ice for 30 min using RIPA buffer supplemented with protease and phosphatase inhibitors. The lysates were centrifuged at 12,000 rpm at 4 °C for 20 min, and the supernatants were collected for protein concentration measurement using a BCA assay. After separation by SDS-PAGE, proteins were transferred to PVDF membranes. The membranes were blocked with 5% non-fat milk in TBST for 1 h at room temperature, followed by incubation with primary antibodies at 4 °C overnight and subsequent incubation with DyLight 800-conjugated secondary antibodies at room temperature for 1 h. Information for the related antibodies is provided in Supplementary Table 2. Protein bands were visualized using an Odyssey fluorescence imaging system (LI-COR) and quantified with ImageJ software. The expression of target proteins was normalized to GAPDH.[26]

Coimmunoprecipitation (Co-IP) and immunoblotting

Co-IP assays were performed to investigate the interaction between TβR-I and Smurf2. Protein lysates were prepared using RIPA buffer supplemented with protease inhibitors. For each sample, 10% of the lysate was reserved as an input control. The remainder was subjected to immunoprecipitation overnight at 4 °C with an anti-TβR-I antibody, using an Antibody Crosslink Immunoprecipitation Kit (Beyotime, Cat. # P2180S) according to the manufacturer's protocol.[31] The immunoprecipitated complexes and input controls were then analyzed by western blotting with antibodies against Smurf2 and TβR-I. To assess TβR-I ubiquitination, LX-2 cells were transfected with an HA-ubiquitin plasmid. Subsequently, cell lysates were immunoprecipitated with an anti-TβR-I antibody, and the ubiquitination level was determined by immunoblotting the precipitates with an anti-HA antibody.

Quantitative RT-PCR

Total RNA was isolated using TRIzol, and 1 μg RNA was reverse-transcribed into cDNA using the PrimeScript RT Reagent Kit (Takara, China; Cat. # RR047A) based on the manufacturer's instructions. Quantitative RT-PCR was performed using an ABI 7500 Real-Time PCR System (Applied Biosystems, USA) with TB Green™ Premix Ex Taq™ II (Takara, Cat. # RR820A) according to the manufacturer's instructions.[32] The primer sequences are listed in Supplementary Table 3. Gene expression was normalized to GAPDH as an internal control and quantified using the $2^{-\Delta\Delta Ct}$ method.

Cell Counting Kit-8 assay

LX-2 cells were seeded in 96-well plates at a density of 5 × 10^3 cells per well and subjected to transfection. At 12, 24, 48, and 72 h post-seeding, cell viability was assessed by adding 10 μL of Cell Counting Kit-8 solution to each well, followed by incubation for 2 h. The absorbance at 450 nm was then measured using a microplate reader (ELX800, BioTek, USA).[33]

Flow cytometry

For cell cycle analysis, cells were harvested, fixed in 80% ice-cold ethanol at 4 °C overnight, and then treated with RNase A at 37 °C for 30 min. Subsequently, the cells were stained with propidium iodide in the dark on ice for 30 min before analysis on a CytoFLEX flow cytometer (Beckman Coulter).[34] Data were processed using ModFit software to determine the cell cycle phase distribution. For apoptosis assessment, cells were resuspended in 100 μL of 1× Annexin V binding buffer and stained with 2.5 μL of Annexin V-FITC and 2.5 μL of propidium iodide for 15 min at room temperature in the dark. Then, 400 μL of additional binding buffer was added, and the samples were immediately analyzed using the CytoFLEX cytometer.[35] Information on the corresponding reagents used in experiments can be found in Supplementary Table 4.

Blood chemistry and cytokine measurement

Peripheral blood was collected from mice and centrifuged at 3,000 rpm for 10 min at 4 °C to obtain serum. Serum levels of alanine aminotransferase and aspartate aminotransferase were measured using commercial enzymatic kits on an automated biochemistry analyzer (Chemray 800, Shenzhen, China). The concentrations of TGF-β1 and IL-6 were determined by enzyme-linked immunosorbent assay using a Rayto RT-6100 microplate reader.

RNA sequencing (RNA-seq) and bioinformatic analysis

RNA-seq was performed on LX-2 cells transfected with either a pcDNA3.1-CTSK plasmid or an empty vector (n = 4 per group). Following total RNA extraction, cDNA libraries were constructed and sequenced on an Illumina NovaSeq platform. Raw reads were processed, and differential expression analysis was conducted on the Novomagic Cloud Platform (Novogene), applying a false discovery rate < 0.05 and |log2(fold change)| ≥ 0.5 as significance thresholds.[36] Significantly differentially expressed genes were subsequently subjected to functional enrichment analysis, including Gene Ontology, Reactome, and Gene Set Enrichment Analysis.

Statistical analysis

Data were presented as the mean ± standard deviation. GraphPad Prism 9.0 (San Diego, CA, USA) was used for data processing and statistical plotting. A t-test was used to compare the differences between two groups, and one-way ANOVA was used for multi-group analysis. All experiments were conducted in triplicate, and the results were considered statistically significant at $p < 0.05$.

Results

CTSK expression is upregulated in fibrotic liver tissues and activated HSCs

To delineate the role of CTSK during fibrogenesis, we first assessed its expression in clinical cohorts. Interrogation of Gene Expression Omnibus datasets revealed that CTSK expression progressively increased with advancing stages of hepatitis B virus-associated liver fibrosis (Fig. 1A). Furthermore, CTSK levels were significantly elevated in human cirrhotic tissues from diverse etiologies, including hepatitis C virus infection and alcohol-related injury, compared to healthy

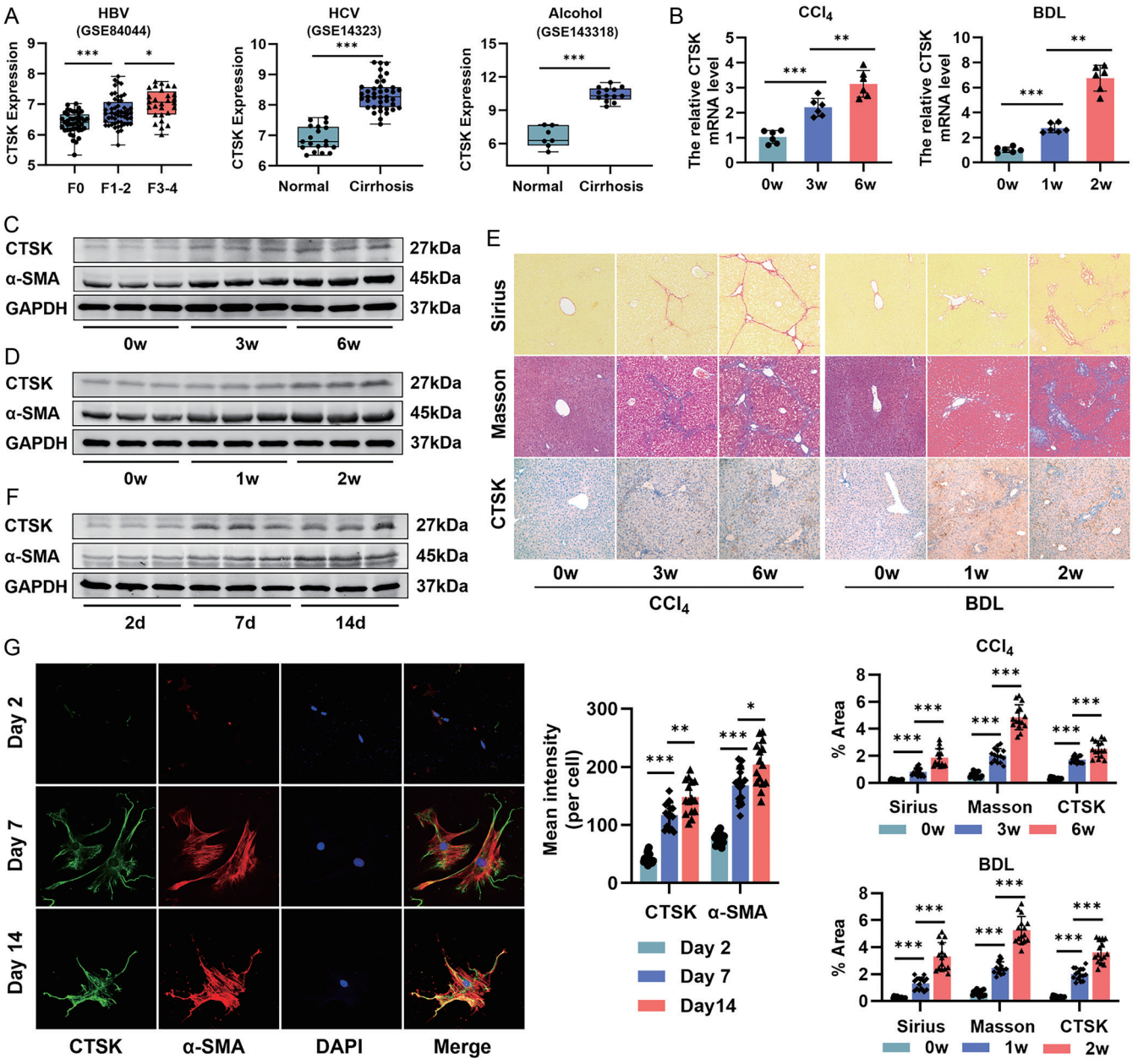

Fig. 1. Analysis of CTSK expression in human and experimental liver fibrosis. (A) Boxplot of *CTSK* expression in liver biopsies from three independent cohorts: across fibrosis stages in HBV-associated cirrhosis (GSE84044); versus healthy controls in HCV-associated cirrhosis (GSE14323); and versus healthy controls in alcohol-associated cirrhosis (GSE143318). (B) qRT-PCR analysis of CTSK mRNA levels in livers from CCl_4-treated mice (at 0, 3, and 6 weeks; left) and BDL-operated mice (at 0, 1, and 2 weeks; right) (n = 6). GAPDH was used as an internal control. (C) and (D) Western blot analysis of CTSK and α-SMA expression in mouse liver fibrosis tissues. Quantification data are shown in Supplementary Fig. 1C and D, respectively (n = 6). (E) Representative images of Sirius Red, Masson's trichrome, and immunohistochemistry for CTSK staining of liver sections from these mice. Quantitative analysis of the positive staining areas. Data are representative of 3 mice (5 random fields per mouse). Magnification, 100×. (F) Western blot analysis of CTSK and α-SMA expression in pHSCs isolated from normal mice and cultured for the indicated times (2, 7, 14 days). Quantification data are shown in Supplementary Fig. 1F (n = 3). (G) Representative immunofluorescence images of pHSCs (from normal mice) cultured for 2, 7, or 14 days, co-stained for CTSK (green) and α-SMA (red). Nuclei are counterstained with DAPI (blue). Data are representative of 3 mice (5 random fields per mouse). Magnification, 200×. $^{*}p < 0.05$; $^{**}p < 0.01$; $^{***}p < 0.001$. All data are illustrated as mean ± SD. CTSK, Cathepsin K; HBV, hepatitis B virus; HCV, hepatitis C virus; qRT-PCR, quantitative reverse transcription polymerase chain reaction; CCl_4, carbon tetrachloride; BDL, bile duct ligation; α-SMA, alpha-smooth muscle actin.

controls (Fig. 1A). We next validated these findings in two established mouse models of liver fibrosis, induced by CCl_4 or BDL. Successful fibrogenesis was confirmed by the upregulation of canonical fibrosis markers (Col1a1, α-SMA, Vimentin; Supplementary Fig. 1A and B) and increased α-SMA protein (Fig. 1C and D; quantifications in Supplementary Fig. 1C and D). Consistent with the human data, both CTSK mRNA and protein levels were markedly increased in fibrotic mouse livers (Fig. 1B–D). Histological analysis demonstrated that the progression of fibrosis, visualized by Sirius Red and Masson's staining, paralleled the upregulation of CTSK (Fig. 1E). Immunohistochemistry localized the elevated CTSK expression

predominantly to the periportal fibrotic regions (Fig. 1E). To confirm that activated HSCs are a major source of CTSK, we analyzed its expression during the spontaneous activation *in vitro* of pHSCs isolated from normal mice (Supplementary Fig. 1E). Western blot analysis revealed a time-dependent upregulation of both α-SMA and CTSK protein during this process (Fig. 1F; quantified in Supplementary Fig. 1F). Immunofluorescence analysis further confirmed that the increase in CTSK expression coincided with the morphological transition to activated, α-SMA-positive myofibroblasts (Fig. 1G). To validate our *in vitro* observations, fibrotic mouse liver sections were stained by dual immunofluorescence for CTSK and the activated HSC marker α-SMA. Significant colocalization was quantified specifically in fibrotic areas, with a Pearson's correlation coefficient of 0.599 ± 0.045. This result demonstrates the specific enrichment of CTSK in activated hepatic stellate cells within the fibrotic liver microenvironment, consistent with the immunohistochemistry findings (Supplementary Fig. 1G and H). Furthermore, analysis of basal CTSK expression across different cell lines, AML12 hepatocytes, RAW 264.7 macrophages, LX-2 cells, and pHSCs, demonstrated markedly higher expression in HSCs compared to hepatocytes and macrophages (Supplementary Fig. 1I and J). Collectively, these data from human tissues, mouse models, and primary cells established that CTSK expression is a conserved feature of liver fibrogenesis.

CTSK overexpression inhibits HSC activation and proliferation in vitro

To obtain a comprehensive profile of CTSK function, we performed RNA-seq on LX-2 cells overexpressing CTSK. This analysis identified 3,428 upregulated and 3,448 downregulated genes (Fig. 2A). Interrogation of a fibrosis-related gene set revealed that CTSK overexpression suppressed the HSC activation signature, which was characterized by the coordinated downregulation of multiple collagens, MMP2, and MMP9, alongside the upregulation of MMP1 and MMP11 (Fig. 2B). We next directly validated this anti-fibrotic activity using gain-of-function approaches. Following efficient overexpression of CTSK in LX-2 cells (via plasmid) and pHSCs (via adenovirus) (Supplementary Fig. 2A and B), we assessed key fibrotic markers. In LX-2 cells, CTSK overexpression significantly downregulated the mRNA and protein levels of COL1A1, α-SMA, and Vimentin, both with and without TGF-β stimulation (Fig. 2C and D; quantification in Supplementary Fig. 2C). This inhibitory effect was consistently recapitulated in pHSCs, as confirmed by Western blot (Fig. 2E; quantification in Supplementary Fig. 2D) and immunofluorescence analyses (Fig. 2F). Furthermore, we investigated whether CTSK impacted HSC proliferation. Flow cytometric cell cycle analysis demonstrated that CTSK overexpression induced G1 phase arrest, evidenced by a significant increase in the proportion of cells in G1 phase (Fig. 2G). Taken together, these data established that CTSK functions as an inhibitor of both HSC activation and proliferation *in vitro*.

CTSK overexpression inhibits the TGF-β/Smad pathway by promoting ubiquitin-mediated degradation of TβR-I

Pathway analysis of the RNA-seq data from CTSK-overexpressing LX-2 cells revealed significant enrichment of differentially expressed genes in the TβR signaling pathway and ubiquitin-mediated proteolysis (Fig. 3A). This prompted us to investigate a potential link between CTSK and TGF-β signaling. Given that TGF-β1 is a potent fibrogenic cytokine,[5] we first confirmed that its treatment of LX-2 cells induced activation and also led to a gradual upregulation of CTSK (Supplementary Fig. 2E), mirroring our earlier findings in activated pHSCs (Fig. 1G). Strikingly, while TGF-β1 treatment activated downstream signaling in LX-2 cells, as evidenced by increased Smad2/3 phosphorylation, CTSK overexpression effectively suppressed this phosphorylation in both LX-2 cells and pHSCs without altering total Smad2/3 levels (Fig. 3B and C; quantifications in Supplementary Fig. 2G and H). This inhibition was functionally confirmed by immunofluorescence, which showed that CTSK overexpression blocked the TGF-β-induced nuclear translocation of p-Smad2/3 in both cell types (Fig. 3D and E). These results indicated that CTSK is a negative regulator involved in TGF-β/Smad signaling. To elucidate the mechanism underlying this suppression of TGF-β signaling, we next examined the effect of CTSK overexpression on TβRs (TβR-I and TβR-II). CTSK overexpression significantly decreased the protein levels of TβR-I but not TβR-II in LX-2 cells (Fig. 3F; quantification in Supplementary Fig. 2I), without a corresponding decrease in TβR-I mRNA (Supplementary Fig. 2J), suggesting a post-translational mechanism for TβR-I downregulation. Pre-treatment of the cells with the proteasome inhibitor MG132 rescued the CTSK-induced downregulation of both TβR-I and the fibrotic markers COL1A1 and α-SMA (Fig. 3G; quantification in Supplementary Fig. 2K). These data collectively demonstrated that CTSK targets TβR-I for ubiquitin-mediated proteasomal degradation, thereby blunting the TGF-β/Smad pathway and subsequent HSC activation.

CTSK overexpression induces the ubiquitin-mediated degradation of TβR-I via the Smad7/Smurf2 axis

The Smad7/Smurf2 axis is an established complex that mediates TβR-I ubiquitination and degradation.[37] We found a significant positive correlation between CTSK and Smad7 expression in human liver fibrosis (Fig. 4A). Accordingly, CTSK overexpression elevated Smad7 protein levels in LX-2 cells (Fig. 4B; quantification in Supplementary Fig. 3A). Furthermore, CTSK overexpression reduced Smurf2 protein levels and promoted its nuclear-to-cytoplasmic relocalization, a hallmark of its activation (Fig. 4B and C). This is consistent with a model wherein activated Smurf2, after ubiquitinating its targets, is itself degraded.[38] To establish a functional requirement for Smad7, we performed knockdown experiments (efficiency confirmed in Supplementary Fig. 3B). Smad7 knockdown reversed the CTSK-mediated degradation of TβR-I and blocked the cytoplasmic translocation of Smurf2 (Fig. 4D and E; quantification in Supplementary Fig. 3C), confirming that Smad7 is essential for both processes. Co-IP experiments directly tested this model. In CTSK-overexpressing cells, the interaction between endogenous Smurf2 and TβR-I was enhanced (Fig. 4F, Supplementary Fig. 3D and E), leading to significantly increased TβR-I ubiquitination (Fig. 4G, Supplementary Fig. 3F and G). Critically, Smad7 knockdown abolished both the enhanced Smurf2/TβR-I interaction and TβR-I ubiquitination (Fig. 4F and G). Collectively, these results demonstrated that CTSK promotes TβR-I ubiquitination and degradation by upregulating Smad7 to assemble and activate the Smurf2-TβR-I complex.

CTSK overexpression induces mitochondrial apoptosis in HSCs by disrupting the Bax/Bcl-2 balance

RNA-seq analysis of CTSK-overexpressing LX-2 cells indicated a profound impact on apoptosis. Both Gene Ontology analysis of apoptotic mitochondrial changes and Gene Set Enrichment Analysis revealed significant enrichment of apoptotic pathways (Fig. 5A and B). Prompted by these findings,

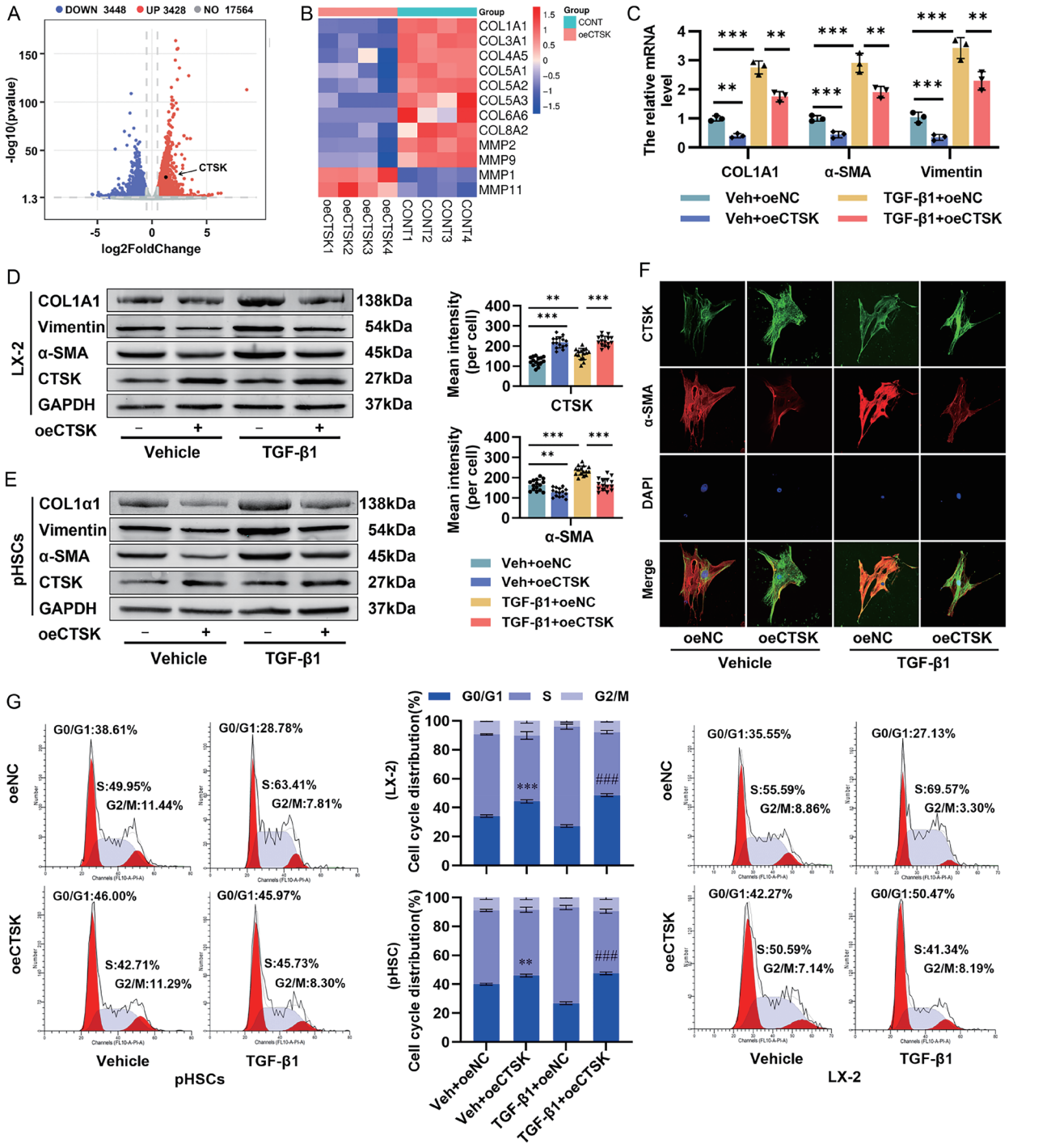

Fig. 2. Effects of CTSK overexpression on HSC activation and proliferation *in vitro*. (A) Volcano plot displaying DEGs from RNA-seq data of LX-2 cells overexpressing CTSK for 48 h (upregulated: 3,428, red; downregulated: 3,448, blue). (B) Heatmap of mRNA expression for fibrosis-related DEGs identified by RNA-seq. (C) qRT-PCR analyses of Col1A1, α-SMA, and vimentin in CTSK-overexpressing LX-2 cells treated with or without TGF-β1 (5 ng/mL) for 24 h (n = 3). GAPDH was used as an internal control. (D) and (E) Western blot analysis of Col1a1, α-SMA, and vimentin in (D) CTSK-overexpressing LX-2 cells and (E) CTSK-overexpressing pHSCs, treated with or without TGF-β1 (5 ng/mL, 24 h) (n = 3). Quantification data are shown in Supplementary Fig. 2C and D. (F) Representative images of double immunofluorescence staining for CTSK (green) and α-SMA (red) in pHSCs following CTSK overexpression and treatment with or without TGF-β1 (5 ng/mL) for 24 h. Nuclei were counterstained with DAPI (blue). Data are representative of 3 mice (5 random fields per mouse). Magnification, 200×. (G) Cell cycle analysis of pHSCs (left) and LX-2 cells (right) overexpressing CTSK and treated with or without TGF-β1 for 24 h. The distribution of cell cycle phases was quantified by flow cytometry with PI staining. Bar graphs show the quantitative results (n = 3). $^{**}p < 0.01$, $^{***}p < 0.001$ vs. oeNC group; $^{\#\#\#}p < 0.001$ vs. TGF-β1 group. $^{**}p < 0.01$; $^{***}p < 0.001$. All data are illustrated as mean ± SD. The symbols "+" and "−" represent groups with or without CTSK overexpression, respectively. CTSK, Cathepsin K; DEGs, differentially expressed genes; qRT-PCR, quantitative reverse transcription polymerase chain reaction; α-SMA, alpha-smooth muscle actin; TGF-β1, transforming growth factor beta 1; pHSCs, primary hepatic stellate cells; PI, propidium iodide.

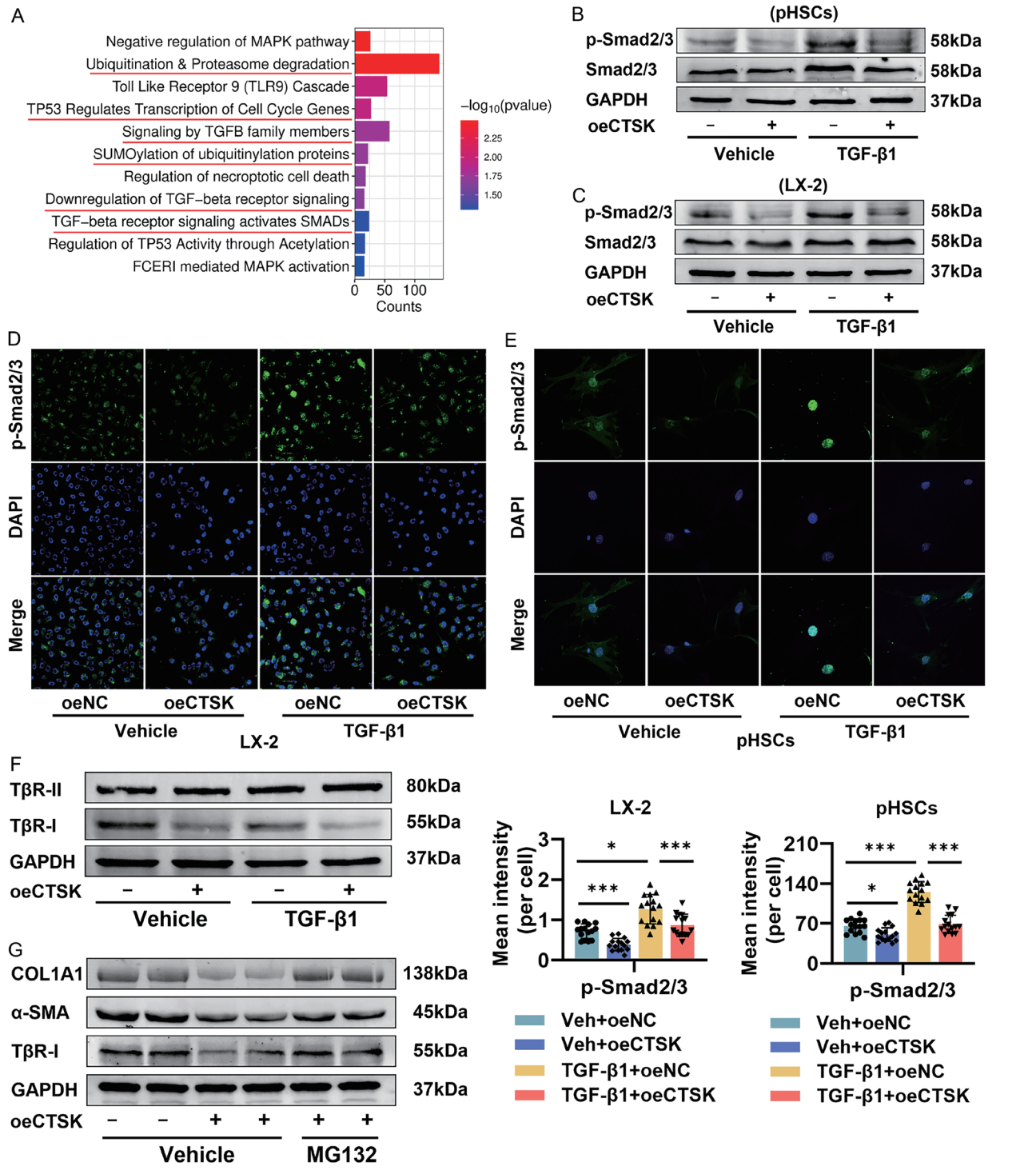

Fig. 3. Effects of CTSK overexpression on the TGF-β/Smad pathway. (A) Reactome pathway analysis of DEGs identified by RNA-seq. (B) and (C) Western blot analysis of Smad2/3 and p-Smad2/3 in (B) pHSCs and (C) LX-2 cells following CTSK overexpression and stimulation with or without TGF-β1 (5 ng/mL, 24 h) (n = 3). Quantification data are shown in Supplementary Fig. 2G and H. (D) and (E) Representative images of immunofluorescence staining for p-Smad2/3 (green) in CTSK-overexpressing LX-2 cells (D) or pHSCs (E) treated with or without TGF-β1 (5 ng/mL) for 24 h. Nuclei were counterstained with DAPI (blue). Quantitative analysis of the mean fluorescence intensity for p-Smad2/3 (N = 3, n = 5 fields/experiment). (F) Western blot analysis of TβR-I and TβR-II in CTSK-overexpressing LX-2 cells treated with or without TGF-β1 for 24 h. Quantification data are shown in Supplementary Fig. 2I (n = 3). (G) Western blot analysis of TβR-I, α-SMA, and COL1A1 protein levels in LX-2 cells overexpressing CTSK and treated with or without the proteasome inhibitor MG132 (10 μM, 4 h) (n = 3). Quantification data are shown in Supplementary Figure 2K (n = 3). ns = not significant. $^{*}p < 0.05$; $^{**}p < 0.01$; $^{***}p < 0.001$. All data are illustrated as mean ± SD. The symbols "+" and "−" represent groups with or without CTSK overexpression, respectively. CTSK, Cathepsin K; DEGs, differentially expressed genes; TGF-β, transforming growth factor beta; TβR-I/II, transforming growth factor-β receptor I/II; pHSCs, primary hepatic stellate cells; α-SMA, alpha-smooth muscle actin.

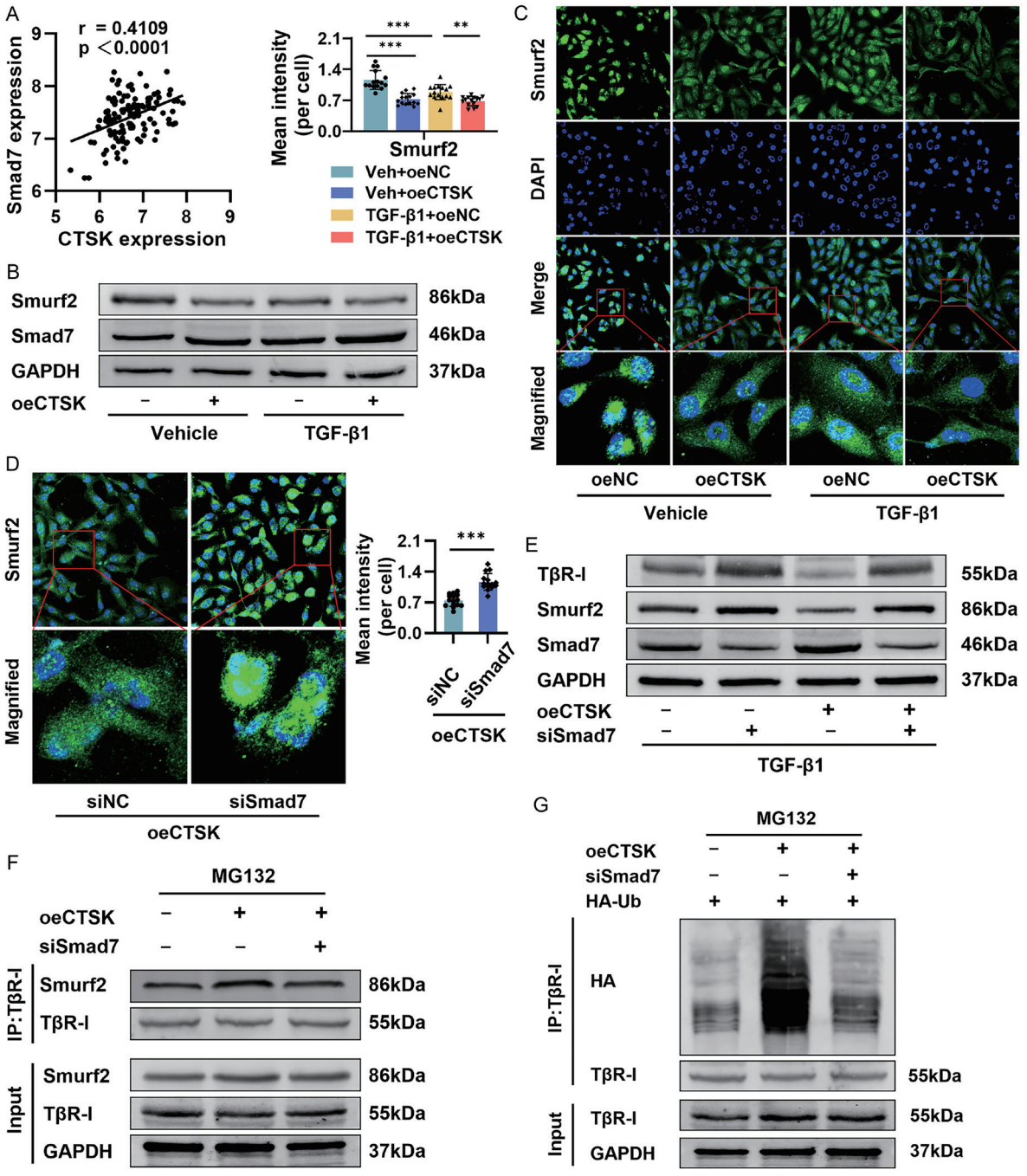

Fig. 4. Effects of CTSK overexpression on Smad7/Smurf2 expression and their interaction with TβR-I. (A) Scatter plot with linear regression fit showing the correlation between CTSK and Smad7 mRNA expression in HBV-associated cirrhosis (GSE84044) (Pearson r = 0.4109, $p < 0.0001$). (B) Western blot analysis of Smad7 and Smurf2 in CTSK-overexpressing LX-2 cells treated with or without TGF-β1 (5 ng/mL) for 24 h. Quantification data are shown in Supplementary Fig. 3A (n = 3). (C) Representative immunofluorescence images of Smurf2 (green) in CTSK-overexpressing LX-2 cells treated with or without TGF-β1 (5 ng/mL) for 24 h, with higher magnification views shown. Nuclei were counterstained with DAPI (blue). Quantitative analysis of the mean fluorescence intensity for Smurf2 (N = 3, n = 5 fields/experiment). Magnification, 200×. (D) Representative immunofluorescence images of Smurf2 (green) in LX-2 cells after CTSK overexpression and Smad7 knockdown for 24 h, with higher magnification views shown. Nuclei were counterstained with DAPI (blue). Quantitative analysis of the mean fluorescence intensity for Smurf2 (N = 3, n = 5 fields/experiment). Magnification, 200×. (E) Western blot analysis of Smad7, Smurf2, and TβR-I in LX-2 cells after CTSK overexpression and Smad7 knockdown followed by TGF-β1 (5 ng/mL) treatment for 24 h (n = 3). Quantification data are shown in Supplementary Fig. 3C. (F) Co-IP analysis of the interaction between TβR-I and Smurf2 in LX-2 cells overexpressing CTSK with or without Smad7 knockdown, and treated with MG132 (10 μM, 4 h) (n = 3). Input lysates are shown in Supplementary Fig. 3D. Quantitative analysis of the binding efficiency is shown in Supplementary Fig. 3E. (G) Ubiquitination assay for TβR-I in LX-2 cells under the same conditions as in (F), co-transfected with an HA-Ubiquitin plasmid and treated with MG132 (10 μM, 4 h) (n = 3). Quantitative analysis of TβR-I ubiquitination levels is shown in Supplementary Fig. 3F. $^{**}p < 0.01$; $^{***}p < 0.001$. All data are illustrated as mean ± SD. The symbols "+" and "−" indicate the presence or absence of the respective treatment (CTSK overexpression, siSmad7, or HA-Ub transfection), respectively. CTSK, Cathepsin K; HBV, hepatitis B virus; TGF-β1, transforming growth factor beta 1; TβR-I, transforming growth factor-β receptor I; Co-IP, co-immunoprecipitation.

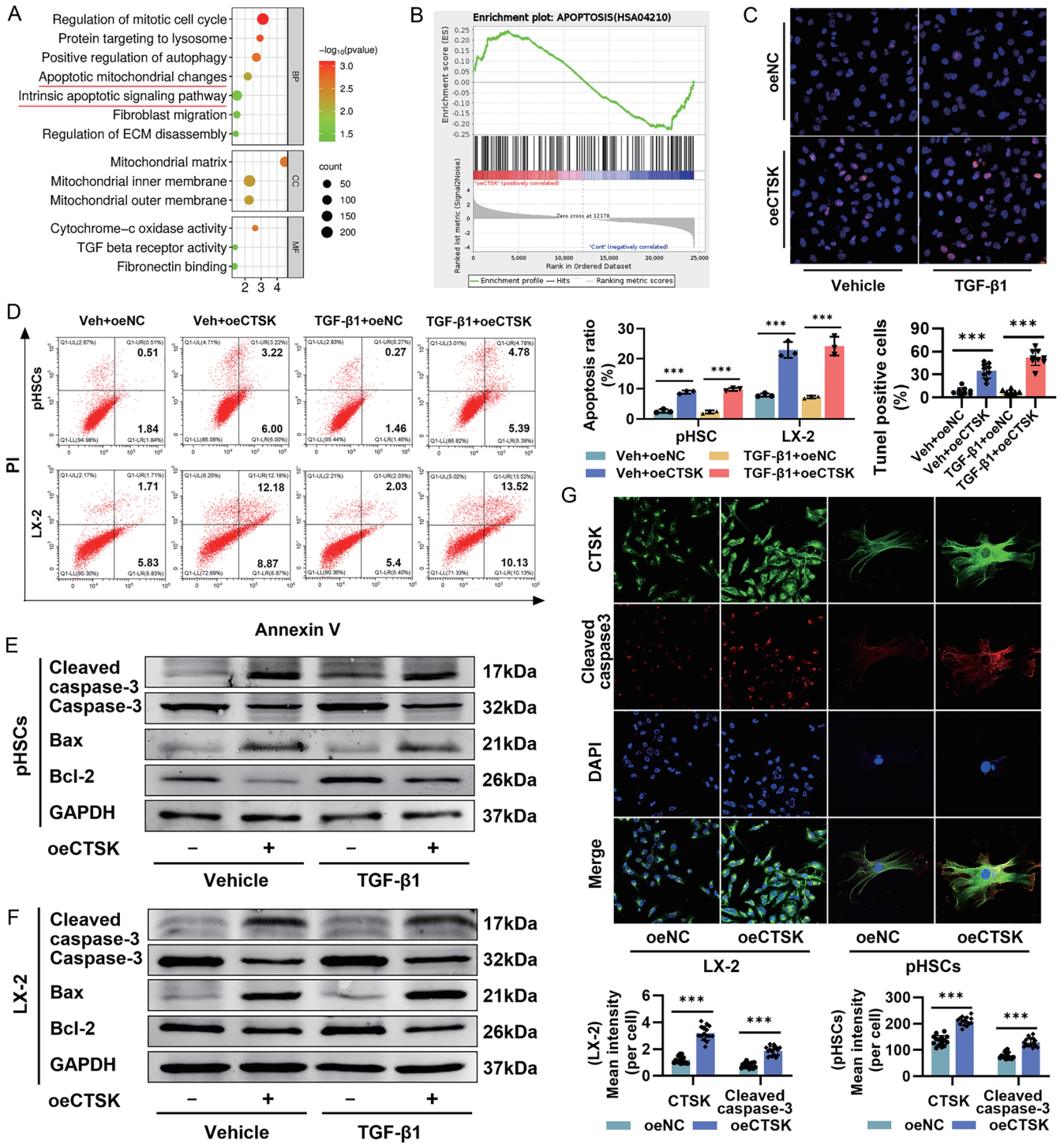

Fig. 5. Analysis of apoptosis and apoptosis-related protein expression in HSCs overexpressing CTSK. (A) Dot plot showing significantly enriched GO terms for DEGs identified by RNA-seq. (B) GSEA shows significant enrichment of the apoptosis gene set. (C) Apoptosis in LX-2 cells with CTSK overexpression was assessed by TUNEL staining after treatment with or without TGF-β1 (5 ng/mL) for 24 h (N = 3, n = 3 fields/experiment). (D) Apoptosis was assessed by flow cytometry in pHSCs and LX-2 cells overexpressing CTSK. Cells were treated with or without TGF-β1 (5 ng/mL) for 24 h (n = 3). (E) and (F) Western blot analysis of the effect of CTSK overexpression on apoptosis-related proteins (Bcl-2, Bax, Caspase-3, and cleaved Caspase-3) in (E) pHSCs and (F) LX-2 cells treated with or without TGF-β1 (5 ng/mL) for 24 h (n = 3). Quantification data are shown in Supplementary Fig. 4C and D, respectively. (G) Representative images of double immunofluorescence staining for CTSK (green) and cleaved Caspase-3 (red) in CTSK-overexpressing LX-2 cells and pHSCs for 24 h. Nuclei were counterstained with DAPI (blue) (N = 3, n = 5 fields/experiment). Magnification, 200×. $^{***}p < 0.001$. All data are illustrated as mean ± SD. The symbols "+" and "−" represent groups with or without CTSK overexpression, respectively. CTSK, Cathepsin K; Bax, Bcl-2-associated X protein; Bcl-2, B-cell lymphoma 2; GO, Gene Ontology; DEGs, differentially expressed genes; GSEA, Gene Set Enrichment Analysis; TGF-β1, transforming growth factor beta 1; pHSCs, primary hepatic stellate cells.

we assessed the functional impact of CTSK on HSC survival. CTSK overexpression significantly increased the proportion of TUNEL-positive LX-2 cells (Fig. 5C). Flow cytometry confirmed that CTSK elevated both early and late apoptotic populations in LX-2 cells and pHSCs (Fig. 5D), culminating in a significant reduction in overall cell viability (Supplementary Fig. 4A and B). We next investigated the mitochondrial apoptotic pathway, where an imbalance between the pro-apoptotic protein Bax and the anti-apoptotic protein Bcl-2 can trigger cell death.[39] CTSK overexpression in both LX-2 cells and pHSCs upregulated Bax, downregulated Bcl-2, and promoted proteolytic activation of caspase-3 (Fig. 5E and F; quantifications in Supplementary Fig. 4C and D). Immunofluorescence further confirmed that CTSK overexpression increased Cleaved caspase-3 levels (Fig. 5G). To determine whether CTSK regulates HSC apoptosis via TGF-β/Smad signaling, a rescue experiment was performed through Smad7 inhibition. Restoration of TGF-β/Smad signaling was confirmed by elevated phosphorylated Smad2/3 levels; however, apoptosis-related protein expression (Bax, Bcl-2, cleaved caspase-3) remained unaltered (Supplementary Fig. 4E and F). Collectively, these data established that CTSK triggers mitochondrial apoptosis in HSCs by shifting the Bax/Bcl-2 balance toward a pro-apoptotic state.

CTSK overexpression attenuates liver fibrosis in vivo across etiologically distinct models

To evaluate the anti-fibrotic efficacy of CTSK *in vivo*, we employed AAV8-mediated gene delivery to overexpress CTSK in two etiologically distinct mouse models: CCl_4-induced toxic injury and BDL-induced cholestasis (Figs. 6A and 7A). Colocalization analysis showed overlap between CTSK-Flag and α-SMA signals, with a Pearson's correlation coefficient of 0.494 ± 0.030 (Supplementary Fig. 5B). Additionally, a subset of CTSK-Flag signal was distributed independently of α-SMA. Successful hepatic CTSK overexpression was confirmed by RT-qPCR (Supplementary Fig. 5C). Both mouse models exhibited robust fibrosis induction, as evidenced by upregulation of key profibrotic markers (α-SMA, Col1a1, Vimentin) at the mRNA (Figs. 6B and 7B) and protein levels (Figs. 6C and 7C; quantified in Supplementary Fig. 5D and F). This fibrotic response was significantly repressed by AAV8-CTSK injection (Figs. 6B and C, 7B and C). Histologically, a considerable reduction of fibrosis was confirmed in AAV8-CTSK-injected mice, as shown by Sirius Red, Masson staining, and Vimentin immunohistochemistry (Figs. 6D and 7D). H&E staining revealed that CTSK overexpression improved overall hepatic histoarchitecture (Figs. 6D and 7D). These histological improvements were paralleled by a significant amelioration of serum biomarkers, including reduced levels of hepatocellular injury markers (alanine aminotransferase, aspartate aminotransferase) and pro-fibrotic mediators (TGF-β1, IL-6) (Figs. 6E and 7E). These results indicated that CTSK overexpression ameliorated CCl_4- and BDL-induced hepatic fibrosis in mice. Following AAV8-CTSK treatment, a significant increase in activated caspase-3 expression was observed, accompanied by clear colocalization with α-SMA (Fig. 7F; quantified in Supplementary Fig. 5G and H), suggesting that CTSK overexpression promotes apoptosis in HSCs, consistent with *in vitro* observations. Furthermore, phosphorylated Smad2/3, TβR-I, and Smurf2 levels were markedly reduced in livers injected with AAV8-CTSK (Figs. 6F and 7G; quantified in Supplementary Fig. 5E and I). These findings demonstrated that *in vivo* overexpression of CTSK suppresses the TGF-β/Smad signaling pathway, collectively establishing CTSK as a negative regulator of TGF-β signaling in mouse models of hepatic fibrosis.

Discussion

CTSK is highly expressed in the fibrotic livers of human patients and mice. Contrary to the conventional perception of its role, our findings redefine CTSK upregulation during fibrosis not as a passive pathological response, but as an activated endogenous protective mechanism.

The persistence of fibrosis following chronic liver injury suggests that the endogenous protective response from upregulated CTSK is insufficient to suppress the pathological process. Critically, in two distinct mouse models of liver fibrosis, we demonstrated that exogenous CTSK overexpression exerted significant anti-fibrotic effects. These effects were primarily mediated through two mechanisms: suppressing the TGF-β/Smad signaling pathway and inducing HSC mitochondrial apoptosis. Together, these results provide a theoretical basis for targeting CTSK as a potential therapeutic strategy for liver fibrosis.

CTSK, a member of the cathepsin protease family, is highly expressed in osteoclasts and activated in the acidic lysosomal environment through cleavage of its proenzyme precursor.[40] While CTSK is well established as a cysteine protease with potent ECM–degrading activity and has been shown to attenuate fibrosis in the heart and lungs by degrading ECM,[18,19] its role in the liver remained incompletely understood. This study shows that CTSK directly inhibits HSC activation and proliferation by suppressing TGF-β signaling, identifying a novel anti-fibrotic mechanism beyond its conventional role in ECM degradation. Interestingly, we demonstrate that TGF-β upregulates the expression of CTSK in HSCs in a time-dependent manner, establishing a negative feedback loop. Mechanistically, CTSK executes this feedback by facilitating the degradation of its key receptor, TβR-I, thereby blocking the transduction of extracellular signals into intracellular events. This finding is consistent with previous research demonstrating that the degradation of TβR-I in HSCs alleviates liver fibrosis.[41] Given the pleiotropic roles of TGF-β in tissue homeostasis,[6] the CTSK-mediated negative feedback through TβR-I degradation constitutes a precisely targeted mechanism that circumvents the systemic adverse effects of broad pathway inhibition.

Evidence shows that CTSK recruits E3 ubiquitin ligases to mediate substrate ubiquitination and degradation, thereby governing distinct biological processes in muscle wasting, hepatocellular carcinoma, and cervical cancer.[15–17] In our study, we demonstrate that CTSK drives the cytoplasmic translocation of the E3 ligase Smurf2 to facilitate its binding to TβR-I, thereby inducing TβR-I ubiquitination and degradation. This finding extends the established role of CTSK in ubiquitin-mediated proteolysis to HSCs and defines a precise, Smurf2-dependent mechanism for inhibiting liver fibrosis. Furthermore, we elucidate that CTSK facilitates the assembly of the Smurf2–TβR-I complex through Smad7, a critical step in the ubiquitination pathway. Smad7, a key negative regulator of the TGF-β pathway, acts through competitive binding to TβR-I to inhibit Smad2/3 phosphorylation.[42] Our experiments demonstrate that Smad7 mediates the cytoplasmic translocation of Smurf2 and promotes its binding to TβR-I in HSCs, consistent with previous studies.[37,43] Knockdown of Smad7 expression inhibited CTSK-induced cytoplasmic translocation of Smurf2 and the ubiquitination and degradation of TβR-I, further confirming the central role of Smad7 in the CTSK-facilitated assembly of the Smurf2–TβR-I complex. Therefore, our study defines a precise Smad7/Smurf2-dependent mechanism in the UPS through which CTSK inhibits TGF-β signaling and liver fibrosis. Given the pleiotropic nature of the UPS,[44,45] our findings suggest that CTSK's function as a regulator of protein stability likely extends beyond

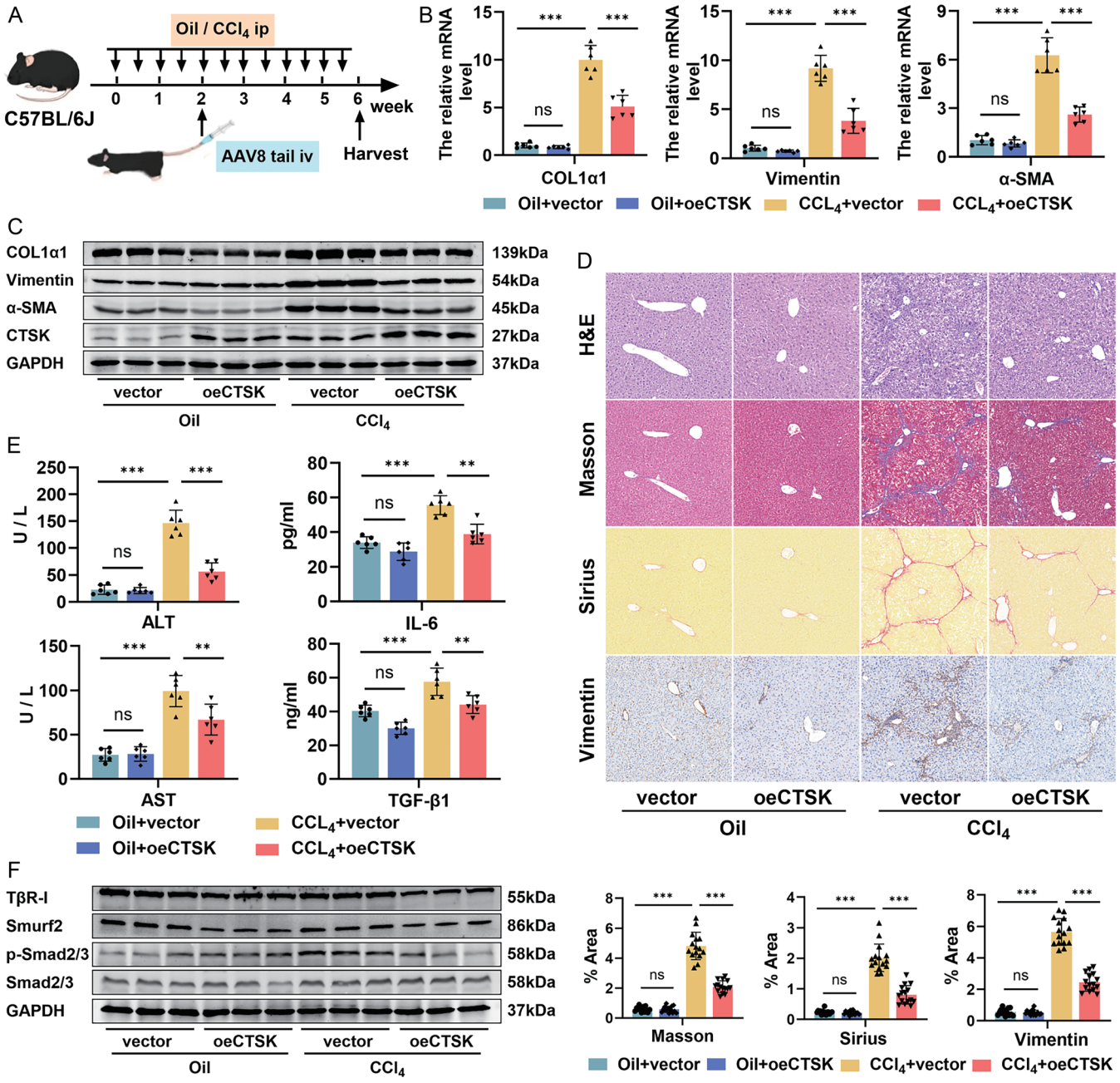

Fig. 6. Analysis of CCl_4-induced liver fibrosis in mice overexpressing CTSK. (A) Schematic diagram of the experimental timeline. (B) qRT-PCR analysis of *Col1a1, vimentin, and α-SMA* in mouse liver tissues (n = 6). GAPDH was used as an internal control. (C) Western blot analysis of Col1a1, vimentin, α-SMA, and CTSK in mouse liver tissues. Quantification data are shown in Supplementary Fig. 5D (n = 6). (D) Representative images of H&E, Masson's trichrome, Sirius Red, and immunohistochemistry for vimentin staining of liver sections. Quantitative analysis of the positive staining areas. Data are representative of 3 mice (5 random fields per mouse). Magnification, 100×. (E) Serum levels of ALT, AST, IL-6, and TGF-β1 in each group (n = 6). (F) Western blot analysis of Smad2/3, p-Smad2/3, Smurf2, and TβR-I in mouse liver tissues (n = 6). Quantification data are shown in Supplementary Fig. 5E. ns = not significant. $^{**}p < 0.01$; $^{***}p < 0.001$. All data are illustrated as mean ± SD. CTSK, Cathepsin K; CCl_4, carbon tetrachloride; qRT-PCR, quantitative reverse transcription polymerase chain reaction; α-SMA, alpha-smooth muscle actin; H&E, hematoxylin and eosin; ALT, alanine aminotransferase; AST, aspartate aminotransferase; IL-6, interleukin-6; TGF-β1, transforming growth factor beta 1.

TβR-I, potentially targeting additional substrates and exerting wider biological influence.

While liver fibrosis was historically viewed as irreversible, recent studies have demonstrated its regression following etiology elimination or effective therapeutic intervention.[46] The apoptosis-resistant phenotype of activated HSCs constitutes a major barrier to fibrosis reversal.[47] Mechanistically, activated HSCs evade apoptosis through two key strategies: maintaining the dominance of the anti-apoptotic protein Bcl-2 and suppressing death receptor signaling.[47,48] Thus, it has been established that inducing apoptosis in activated HSCs is a promising therapeutic strategy to reverse liver fibrosis.[49,50] Given that the lysosomal protease CTSK can proteolytically regulate Bcl-2 family members,[51,52] we investigated its role

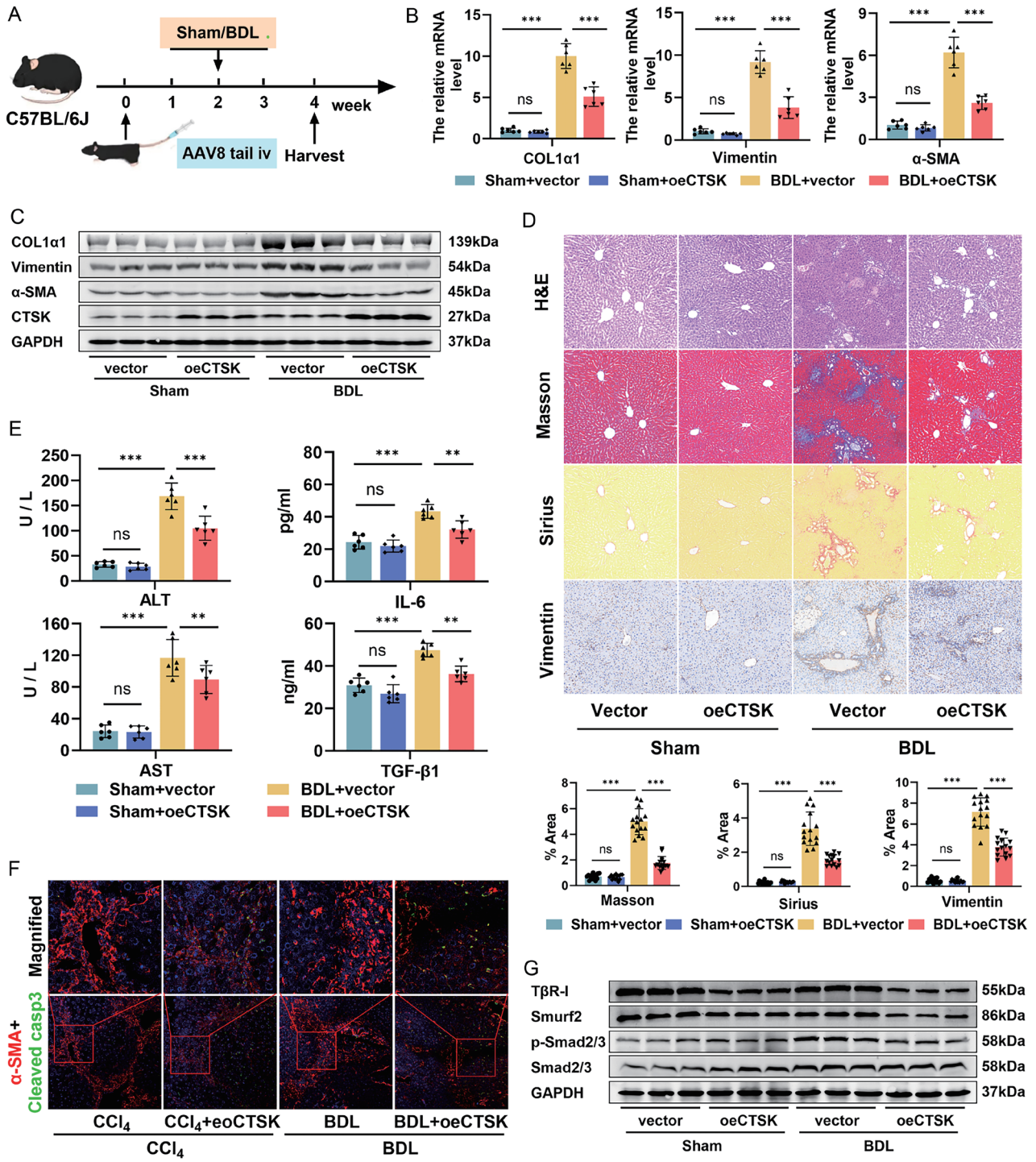

Fig. 7. Analysis of BDL-induced cholestatic fibrosis in mice overexpressing CTSK. (A) Schematic diagram of the experimental timeline. (B) qRT-PCR analysis of *Col1a1, vimentin, and α-SMA* in mouse liver tissues (n = 6). GAPDH was used as an internal control. (C) Western blot analysis of Col1a1, vimentin, α-SMA, and CTSK in mouse liver tissues (n = 6). Quantification data are shown in Supplementary Fig. 5F. (D) Representative images of H&E, Sirius Red, Masson's trichrome, and immunohistochemistry for vimentin staining of liver sections. Quantitative analysis of the positive staining areas. Data are representative of 3 mice (5 random fields per mouse). Magnification, 100×. (E) Serum levels of ALT, AST, IL-6, and TGF-β1 in each group (n = 6). (F) Representative immunofluorescence images of dual staining for cleaved Caspase-3 (green) and α-SMA (red) in fibrotic liver tissues from BDL- and CCl_4-induced mouse models. Nuclei are counterstained with DAPI (blue). Magnification, 200×. Data are representative of 3 mice (3 random fields per mouse). Quantification data are shown in Supplementary Fig. 5G and H. (G) Western blot analysis of Smad2/3, p-Smad2/3, Smurf2, and TβR-I in mouse liver tissues (n = 6). Quantification data are shown in Supplementary Fig. 5I. ns = not significant. $^{**}p < 0.01$; $^{***}p < 0.001$. All data are illustrated as mean ± SD. CTSK, Cathepsin K; BDL, bile duct ligation; qRT-PCR, quantitative reverse transcription polymerase chain reaction; α-SMA, alpha-smooth muscle actin; H&E, hematoxylin and eosin; ALT, alanine aminotransferase; AST, aspartate aminotransferase; IL-6, interleukin-6; TGF-β1, transforming growth factor beta 1.

in HSC fate determination. Collectively, our data demonstrate that CTSK shifts the HSC survival–apoptosis balance toward apoptosis by modulating the Bax/Bcl-2 ratio. This pro-apoptotic effect, which promotes the clearance of pathological myofibroblasts *in vitro* and aligns with prior findings,[20] was critically validated *in vivo*. In two independent animal models, CTSK overexpression potently enhanced the apoptosis of activated HSCs within established fibrotic niches, confirming the therapeutic relevance of this mechanism in a pathophysiological context. TGF-β regulates diverse cellular processes, including cell fate decisions, through crosstalk with other signaling pathways.[53] Our rescue experiments using Smad7 inhibition demonstrate that CTSK's suppression of this pathway is functionally independent of its ability to induce Bax/Bcl-2 imbalance. This dual and independent action enables CTSK to simultaneously attenuate a key pro-fibrotic survival signal (TGF-β) and directly activate apoptosis in HSCs. Consequently, targeting CTSK presents a rational strategy to counteract both HSC activation and persistence, supporting its potential as a therapeutic approach for reversing liver fibrosis.

The diverse etiology and complex nature of liver fibrosis hamper its successful translation from bench to bedside. In this context, the broad-spectrum anti-fibrotic efficacy of CTSK in both CCl4- and BDL-induced liver fibrosis models underscores its promising clinical translational potential. Moreover, its consistent upregulation across diverse fibrotic conditions, particularly within activated HSCs, positions CTSK as a strong candidate for a disease progression biomarker; this hypothesis warrants further clinical investigation. While systemic CTSK inhibition has proven effective in osteoporosis and rheumatoid arthritis,[54,55] our findings raise concerns by revealing that the same strategy could inadvertently exacerbate liver fibrosis. This potential adverse effect, contrasting with its beneficial role in other diseases, underscores that the net effect of CTSK modulation is highly tissue-specific. Therefore, translating these insights will require a paradigm shift from broad systemic inhibition to tissue-specific or pathway-precise targeting, achievable by developing advanced delivery systems that maximize efficacy and minimize off-target risks.

Our study establishes a significant role for CTSK in inhibiting liver fibrosis, yet it has several limitations. First, while the gain-of-function approach defines the therapeutic potential of CTSK, it cannot fully elucidate the physiological functions of the endogenous protein. Second, while our AAV8-mediated overexpression of CTSK successfully targeted HSCs and elicited the expected biological effects, the inherent tropism of AAV8 for multiple liver cell types means this approach lacks definitive cellular specificity. Consequently, future studies employing HSC-specific promoters and conditional knockout models will be essential to: (i) definitively confirm the cell-autonomous functions of CTSK within HSCs, and (ii) decipher its potential paracrine or broader signaling roles in hepatic intercellular crosstalk. A key translational consideration stems from the difference between experimental models and human disease: the cellular specificity of CTSK upregulation in human fibrotic livers remains undefined. Conclusively mapping CTSK-expressing cells in patient tissues using spatial transcriptomics is therefore essential to validate the clinical relevance of our findings. Furthermore, our findings prompt important questions regarding long-term therapeutic strategy. A recent study revealed that CTSK has dual roles in pulmonary fibrosis: its early elevation inhibits fibrosis by degrading ECM, whereas sustained elevation pathologically activates glutamine metabolism to exacerbate fibrosis.[56] Given this finding, the long-term efficacy, systemic safety, and potential side effects of sustained CTSK expression in our liver fibrosis models remain a critical area for future investigation.

Conclusions

Our study demonstrates that CTSK ameliorates hepatic fibrosis through dual mechanisms: suppression of the TGF-β/Smad pathway via a Smad7/Smurf2-dependent ubiquitination mechanism, and direct disruption of the apoptosis-resistant barrier in HSCs. This work extends the role of CTSK beyond that of a conventional ECM-degrading enzyme to a key regulator of protein homeostasis and cell fate. As a multifunctional regulatory protein, CTSK presents a promising therapeutic target warranting further exploration for the treatment of liver fibrosis.

Acknowledgments

We acknowledge Figdraw for its assistance in creating the graphical abstract.

Funding

The work was supported by the National Natural Science Foundation of China (grant number 81970504); the Natural Science Foundation of Hebei Province (grant number H2018206326); the Key Research and Development Program of Hebei Province (grant number 19277779D); the Medical Talents Program of Hebei Province (2021); and the Fourth Batch of Top-talents of Hebei Province.

Conflict of interest

YN has been an Editorial Board Member of *Journal of Clinical and Translational Hepatology* since 2022. The other authors have no conflicts of interest related to this publication.

Author contributions

Study concept and design (ZL), analysis and interpretation of data (MS, DZ, YM), performing the experiments (ZL, YS, JC, CZ, YZ), manuscript preparation (ZL, YC), study supervision (YZ, QZ, SL), and critical revision of the manuscript for important intellectual content (YN). All authors have made significant contributions to this study and have approved the final manuscript.

Ethical statement

The research protocol was approved and supervised by the Ethics Committee of the Third Hospital of Hebei Medical University (approval number: Z2024-030-1). All animals received humane care.

Data sharing statement

All data are available from the corresponding author upon reasonable request.

References

[1] Weiskirchen R. Exploring Molecular Mechanisms of Liver Fibrosis. Int J Mol Sci 2025;26(1):326. doi:10.3390/ijms26010326, PMID:39796182.
[2] Zamani M, Alizadeh-Tabari S, Ajmera V, Singh S, Murad MH, Loomba R. Global Prevalence of Advanced Liver Fibrosis and Cirrhosis in the General Population: A Systematic Review and Meta-analysis. Clin Gastroenterol Hepatol 2025;23(7):1123–1134. doi:10.1016/j.cgh.2024.08.020, PMID:39209202.
[3] Yang X, Li Q, Liu W, Zong C, Wei L, Shi Y, *et al*. Mesenchymal stromal

cells in hepatic fibrosis/cirrhosis: from pathogenesis to treatment. Cell Mol Immunol 2023;20(6):583–599. doi:10.1038/s41423-023-00983-5, PMID: 36823236.
[4] Yan M, Cui Y, Xiang Q. Metabolism of hepatic stellate cells in chronic liver diseases: emerging molecular and therapeutic interventions. Theranostics 2025;15(5):1715–1740. doi:10.7150/thno.106597, PMID:39897543.
[5] Massagué J, Sheppard D. TGF-β signaling in health and disease. Cell 2023; 186(19):4007–4037. doi:10.1016/j.cell.2023.07.036, PMID:37714133.
[6] Peng D, Fu M, Wang M, Wei Y, Wei X. Targeting TGF-β signal transduction for fibrosis and cancer therapy. Mol Cancer 2022;21(1):104. doi:10.1186/s12943-022-01569-x, PMID:35461253.
[7] Ong CH, Tham CL, Harith HH, Firdaus N, Israf DA. TGF-β-induced fibrosis: A review on the underlying mechanism and potential therapeutic strategies. Eur J Pharmacol 2021;911:174510. doi:10.1016/j.ejphar.2021.174510, PMID:34560077.
[8] Park JS, Ma H, Roh YS. Ubiquitin pathways regulate the pathogenesis of chronic liver disease. Biochem Pharmacol 2021;193:114764. doi:10.1016/j.bcp.2021.114764, PMID:34529948.
[9] Hiraiwa M, Fukasawa K, Iezaki T, Sabit H, Horie T, Tokumura K, *et al*. SMURF2 phosphorylation at Thr249 modifies glioma stemness and tumorigenicity by regulating TGF-β receptor stability. Commun Biol 2022;5(1):22. doi:10.1038/s42003-021-02950-0, PMID:35017630.
[10] Zou J, Zhou X, Ma Y, Yu R. Losartan ameliorates renal interstitial fibrosis through metabolic pathway and Smurfs-TGF-β/Smad. Biomed Pharmacother 2022;149:112931. doi:10.1016/j.biopha.2022.112931, PMID: 36068784.
[11] Lotinun S, Ishihara Y, Nagano K, Kiviranta R, Carpentier VT, Neff L, *et al*. Cathepsin K-deficient osteocytes prevent lactation-induced bone loss and parathyroid hormone suppression. J Clin Invest 2019;129(8):3058–3071. doi:10.1172/JCI122936, PMID:31112135.
[12] Sina C, Lipinski S, Gavrilova O, Aden K, Rehman A, Till A, *et al*. Extracellular cathepsin K exerts antimicrobial activity and is protective against chronic intestinal inflammation in mice. Gut 2013;62(4):520–530. doi:10.1136/gutjnl-2011-300076, PMID:22442160.
[13] Funicello M, Novelli M, Ragni M, Vottari T, Cocuzza C, Soriano-Lopez J, *et al*. Cathepsin K null mice show reduced adiposity during the rapid accumulation of fat stores. PLoS One 2007;2(8):e683. doi:10.1371/journal.pone.0000683, PMID:17668061.
[14] Jaffer FA, Kim DE, Quinti L, Tung CH, Aikawa E, Pande AN, *et al*. Optical visualization of cathepsin K activity in atherosclerosis with a novel, protease-activatable fluorescence sensor. Circulation 2007;115(17):2292–2298. doi:10.1161/CIRCULATIONAHA.106.660340, PMID:17420353.
[15] Meng X, Huang Z, Inoue A, Wang H, Wan Y, Yue X, *et al*. Cathepsin K activity controls cachexia-induced muscle atrophy via the modulation of IRS1 ubiquitination. J Cachexia Sarcopenia Muscle 2022;13(2):1197–1209. doi:10.1002/jcsm.12919, PMID:35098692.
[16] Zhang C, Liu Z, Wang X, Zhang B, Cui L, Hu Q, *et al*. Cathepsin K promotes the proliferation of hepatocellular carcinoma cells through induction of SIAH1 ubiquitination and degradation. iScience 2023;26(6):106852. doi:10.1016/j.isci.2023.106852, PMID:37250786.
[17] Mou J, Zheng W, Wei D, Li D, Fan R, Tang Q. CD200-CD200R affects cisplatin and paclitaxel sensitivity by regulating cathepsin K-mediated p65 NF-κB signaling in cervical cancer. Heliyon 2023;9(8):e19220. doi:10.1016/j.heliyon.2023.e19220, PMID:37654464.
[18] Fang W, He A, Xiang MX, Lin Y, Wang Y, Li J, *et al*. Cathepsin K-deficiency impairs mouse cardiac function after myocardial infarction. J Mol Cell Cardiol 2019;127:44–56. doi:10.1016/j.yjmcc.2018.11.010, PMID:30465799.
[19] Srivastava M, Steinwede K, Kiviranta R, Morko J, Hoymann HG, Länger F, *et al*. Overexpression of cathepsin K in mice decreases collagen deposition and lung resistance in response to bleomycin-induced pulmonary fibrosis. Respir Res 2008;9(1):54. doi:10.1186/1465-9921-9-54, PMID:18638383.
[20] Yue X, Piao L, Wang H, Huang Z, Meng X, Sasaki T, *et al*. Cathepsin K Deficiency Prevented Kidney Damage and Dysfunction in Response to 5/6 Nephrectomy Injury in Mice With or Without Chronic Stress. Hypertension 2022;79(8):1713–1723. doi:10.1161/HYPERTENSIONAHA.122.19137, PMID:35726642.
[21] Wang J, Li N, Cang X, Liu X, Gao R, Xu L, *et al*. Identification of CTSK as a TLR-related critical biomarker in liver cirrhosis via integrative bioinformatics and pathological characterization. Sci Rep 2025;15(1):25895. doi:10.1038/s41598-025-11606-6, PMID:40670571.
[22] Wu Y, Yin AH, Sun JT, Xu WH, Zhang CQ. Angiotensin-converting enzyme 2 improves liver fibrosis in mice by regulating autophagy of hepatic stellate cells. World J Gastroenterol 2023;29(33):4975–4990. doi:10.3748/wjg.v29.i33.4975, PMID:37732000.
[23] Rao J, Wang H, Ni M, Wang Z, Wang Z, Wei S, *et al*. FSTL1 promotes liver fibrosis by reprogramming macrophage function through modulating the intracellular function of PKM2. Gut 2022;71(12):2539–2550. doi:10.1136/gutjnl-2021-325150, PMID:35140065.
[24] Martin K, Pritchett J, Llewellyn J, Mullan AF, Athwal VS, Dobie R, *et al*. PAK proteins and YAP-1 signalling downstream of integrin beta-1 in myofibroblasts promote liver fibrosis. Nat Commun 2016;7:12502. doi:10.1038/ncomms12502, PMID:27535340.
[25] Mederacke I, Dapito DH, Affò S, Uchinami H, Schwabe RF. High-yield and high-purity isolation of hepatic stellate cells from normal and fibrotic mouse livers. Nat Protoc 2015;10(2):305–315. doi:10.1038/nprot.2015.017, PMID:25612230.
[26] Yuan X, Li L, Zhang Y, Ai R, Li D, Dou Y, *et al*. Heme oxygenase 1 alleviates nonalcoholic steatohepatitis by suppressing hepatic ferroptosis. Lipids Health Dis 2023;22(1):99. doi:10.1186/s12944-023-01855-7, PMID:37422643.
[27] Lee JH, Jang EJ, Seo HL, Ku SK, Lee JR, Shin SS, *et al*. Sauchinone attenuates liver fibrosis and hepatic stellate cell activation through TGF-β/Smad signaling pathway. Chem Biol Interact 2014;224:58–67. doi:10.1016/j.cbi.2014.10.005, PMID:25451574.
[28] Guo R, Jia X, Ding Z, Wang G, Jiang M, Li B, *et al*. Loss of MLKL ameliorates liver fibrosis by inhibiting hepatocyte necroptosis and hepatic stellate cell activation. Theranostics 2022;12(11):5220–5236. doi:10.7150/thno.71400, PMID:35836819.
[29] Yao H, Song W, Cao R, Ye C, Zhang L, Chen H, *et al*. An EGFR/HER2-targeted conjugate sensitizes gemcitabine-sensitive and resistant pancreatic cancer through different SMAD4-mediated mechanisms. Nat Commun 2022;13(1):5506. doi:10.1038/s41467-022-33037-x, PMID:36127339.
[30] Moreno-Echeverri AM, Susnik E, Vanhecke D, Taladriz-Blanco P, Balog S, Petri-Fink A, *et al*. Pitfalls in methods to study colocalization of nanoparticles in mouse macrophage lysosomes. J Nanobiotechnology 2022;20(1):464. doi:10.1186/s12951-022-01670-9, PMID:36309696.
[31] Feng Y, Han Y, Hu A, Qu Y, Hu Y, Wu H, *et al*. Heliangin acts as a covalent ligand of RPS2 that disrupts pre-rRNA metabolic processes in NPM1-mutated acute myeloid leukemia. Acta Pharm Sin B 2023;13(2):598–617. doi:10.1016/j.apsb.2022.10.018, PMID:36873185.
[32] Li L, Ai R, Yuan X, Dong S, Zhao D, Sun X, *et al*. LINC00886 Facilitates Hepatocellular Carcinoma Tumorigenesis by Sequestering microRNA-409-3p and microRNA-214-5p. J Hepatocell Carcinoma 2023;10:863–881. doi:10.2147/JHC.S410891, PMID:37313303.
[33] Li Y, Xu B, Ren X, Wang L, Xu Y, Zhao Y, *et al*. Inhibition of CISD2 promotes ferroptosis through ferritinophagy-mediated ferritin turnover and regulation of p62-Keap1-NRF2 pathway. Cell Mol Biol Lett 2022;27(1):81. doi:10.1186/s11658-022-00383-z, PMID:36180832.
[34] Jiang Y, Xiang C, Zhong F, Zhang Y, Wang L, Zhao Y, *et al*. Histone H3K27 methyltransferase EZH2 and demethylase JMJD3 regulate hepatic stellate cells activation and liver fibrosis. Theranostics 2021;11(1):361–378. doi:10.7150/thno.46360, PMID:33391480.
[35] Sun M, Wu X, Lin Z, Zhang C, Cui J, Mao Y, *et al*. Investigation of HO-1 Regulation of Liver Fibrosis Related to Nonalcoholic Fatty Liver Disease Through the SIRT1/TGF-ß/Smad3 Pathway. J Clin Transl Hepatol 2025;13(6):456–468. doi:10.14218/JCTH.2024.00481, PMID:40474887.
[36] Zhang Z, Guo M, Li Y, Shen M, Kong D, Shao J, *et al*. RNA-binding protein ZFP36/TTP protects against ferroptosis by regulating autophagy signaling pathway in hepatic stellate cells. Autophagy 2020;16(8):1482–1505. doi:10.1080/15548627.2019.1687985, PMID:31679460.
[37] Ebisawa T, Fukuchi M, Murakami G, Chiba T, Tanaka K, Imamura T, *et al*. Smurf1 interacts with transforming growth factor-beta type I receptor through Smad7 and induces receptor degradation. J Biol Chem 2001; 276(16):12477–12480. doi:10.1074/jbc.C100008200, PMID:11278251.
[38] Malonis RJ, Fu W, Jelcic MJ, Thompson M, Canter BS, Tsikitis M, *et al*. RNF11 sequestration of the E3 ligase SMURF2 on membranes antagonizes SMAD7 down-regulation of transforming growth factor β signaling. J Biol Chem 2017;292(18):7435–7451. doi:10.1074/jbc.M117.783662, PMID:28292929.
[39] Czabotar PE, Garcia-Saez AJ. Mechanisms of BCL-2 family proteins in mitochondrial apoptosis. Nat Rev Mol Cell Biol 2023;24(10):732–748. doi:10.1038/s41580-023-00629-4, PMID:37438560.
[40] Zou N, Liu R, Li C. Cathepsin K(+) Non-Osteoclast Cells in the Skeletal System: Function, Models, Identity, and Therapeutic Implications. Front Cell Dev Biol 2022;10:818462. doi:10.3389/fcell.2022.818462, PMID:35912093.
[41] Feng J, Xu M, Wang J, Zhou S, Liu Y, Liu S, *et al*. Sequential delivery of nanoformulated α-mangostin and triptolide overcomes permeation obstacles and improves therapeutic effects in pancreatic cancer. Biomaterials 2020;241:119907. doi:10.1016/j.biomaterials.2020.119907, PMID: 32120315.
[42] Martin L, Gabbiani G, De Meyer GRY. SMAD7: riding on fibrosis-limiting routes and beyond. EMBO Mol Med 2025;17(9):2180–2190. doi:10.1038/s44321-025-00283-7, PMID:40745212.
[43] Kavsak P, Rasmussen RK, Causing CG, Bonni S, Zhu H, Thomsen GH, *et al*. Smad7 binds to Smurf2 to form an E3 ubiquitin ligase that targets the TGF beta receptor for degradation. Mol Cell 2000;6(6):1365–1375. doi:10.1016/s1097-2765(00)00134-9, PMID:11163210.
[44] Cruz Walma DA, Chen Z, Bullock AN, Yamada KM. Ubiquitin ligases: guardians of mammalian development. Nat Rev Mol Cell Biol 2022;23(5):350–367. doi:10.1038/s41580-021-00448-5, PMID:35079164.
[45] Sherpa D, Chrustowicz J, Schulman BA. How the ends signal the end: Regulation by E3 ubiquitin ligases recognizing protein termini. Mol Cell 2022;82(8):1424–1438. doi:10.1016/j.molcel.2022.02.004, PMID:35247307.
[46] Friedman SL, Pinzani M. Hepatic fibrosis 2022: Unmet needs and a blueprint for the future. Hepatology 2022;75(2):473–488. doi:10.1002/hep.32285, PMID:34923653.
[47] Kisseleva T, Brenner D. Molecular and cellular mechanisms of liver fibrosis and its regression. Nat Rev Gastroenterol Hepatol 2021;18(3):151–166. doi:10.1038/s41575-020-00372-7, PMID:33128017.
[48] Novo E, Marra F, Zamara E, Valfrè di Bonzo L, Monitillo L, Cannito S, *et al*. Overexpression of Bcl-2 by activated human hepatic stellate cells: resistance to apoptosis as a mechanism of progressive hepatic fibrogenesis in humans. Gut 2006;55(8):1174–1182. doi:10.1136/gut.2005.082701, PMID:16423888.
[49] Du K, Maeso-Díaz R, Oh SH, Wang E, Chen T, Pan C, *et al*. Targeting YAP-mediated HSC death susceptibility and senescence for treatment of liver fibrosis. Hepatology 2023;77(6):1998–2015. doi:10.1097/HEP.0000000000000326, PMID:36815382.
[50] Koda Y, Teratani T, Chu PS, Hagihara Y, Mikami Y, Harada Y, *et al*. CD8(+)

tissue-resident memory T cells promote liver fibrosis resolution by inducing apoptosis of hepatic stellate cells. Nat Commun 2021;12(1):4474. doi:10.1038/s41467-021-24734-0, PMID:34294714.
[51] Droga-Mazovec G, Bojic L, Petelin A, Ivanova S, Romih R, Repnik U, *et al*. Cysteine cathepsins trigger caspase-dependent cell death through cleavage of bid and antiapoptotic Bcl-2 homologues. J Biol Chem 2008;283(27):19140–19150. doi:10.1074/jbc.M802513200, PMID:18469004.
[52] Cirman T, Oresić K, Mazovec GD, Turk V, Reed JC, Myers RM, *et al*. Selective disruption of lysosomes in HeLa cells triggers apoptosis mediated by cleavage of Bid by multiple papain-like lysosomal cathepsins. J Biol Chem 2004;279(5):3578–3587. doi:10.1074/jbc.M308347200, PMID:14581476.
[53] Zhu W, Cui Y, Qiu J, Zhang X, Gao Y, Shang Z, *et al*. Exploring the Therapeutic Potential of TGF-β Inhibitors for Liver Fibrosis: Targeting Multiple Signaling Pathways. J Clin Transl Hepatol 2025;13(7):588–598. doi:10.14218/JCTH.2025.00029, PMID:40937077.
[54] Brizuela L, Buchet R, Bougault C, Mebarek S. Cathepsin K Inhibitors as Potential Drugs for the Treatment of Osteoarthritis. Int J Mol Sci 2025;26(7):2896. doi:10.3390/ijms26072896, PMID:40243480.
[55] Yasuda Y, Kaleta J, Brömme D. The role of cathepsins in osteoporosis and arthritis: rationale for the design of new therapeutics. Adv Drug Deliv Rev 2005;57(7):973–993. doi:10.1016/j.addr.2004.12.013, PMID:15876399.
[56] Chen M, Meng X, Zhu Y, Wang D, Wang M, Wang Z, *et al*. Cathepsin K Aggravates Pulmonary Fibrosis Through Promoting Fibroblast Glutamine Metabolism and Collagen Synthesis. Adv Sci (Weinh) 2025;12(34):e13017. doi:10.1002/advs.202413017, PMID:40605618.